Growth of a semi-flexible polymer close to a fluctuating obstacle: application to cytoskeletal actin fibres and testing of ratchet models

2006 J. Phys.: Condens. Matter 18 S357

(http://iopscience.iop.org/0953-8984/18/14/S17)

INSTITUTE OF PHYSICS PUBLISHING JOURNAL OF PHYSICS: CONDENSED MATTER

J. Phys.: Condens. Matter **18** (2006) S357–S374 doi:10.1088/0953-8984/18/14/S17

Growth of a semi-flexible polymer close to a fluctuating obstacle: application to cytoskeletal actin fibres and testing of ratchet models

N J Burroughs and D Marenduzzo

Mathematics Institute, University of Warwick, Coventry CV4 7AL, UK

E-mail: njb@maths.warwick.ac.uk and davide@maths.warwick.ac.uk

Received 30 September 2005
Published 24 March 2006
Online at stacks.iop.org/JPhysCM/18/S357

Abstract

We consider the growth of a semiflexible clamped polymer, or fibre, incident at an angle on a fluctuating two-dimensional obstacle moving against an applied load. This system models a cytoskeletal actin fibre close to a fluctuating membrane or to a diffusing obstacle, such as an artificial bead or a bacterium moving in the cytosol of the host, and under actin polymerization. We review the existing semi-analytic theories and their predictions, and compare them with the results of three-dimensional Monte Carlo dynamic simulations. This allows us to separate the effect of tip and obstacle diffusion on the overall motion. We characterize the statistics of pushing catastrophes, which occur when the fibre tip loses contact with the obstacle and the fibre grows away from or parallel to the obstacle. We discuss the effect of changing the polymerization and depolymerization rates at the fibre tip, which controls the stalling force needed to stop fibre growth, on the obstacle motion. We also consider how our results are modified if the fibres are bundled via attractive interactions, as is believed to be the case in filopodia, and if the wall becomes 'soft', which should better represent a fluctuating and diffusing membrane patch. We find that in both these cases the obstacle moves at a larger speed than predicted by the ratchet model, and we pinpoint the physical mechanisms leading to this velocity enhancement.

(Some figures in this article are in colour only in the electronic version)

1. Introduction

Actin polymerization is a key process in the motility of most cells and of certain kinds of bacteria. In eukaryotic cells, the cytoskeleton can be thought of as a dynamic network of branching semiflexible polymers—actin fibres—which are growing by polymerization close to the cellular membrane. This polymerization deforms the membrane locally into a variety

of well-documented shapes, the most common of which are lamellipodia and filopodia, both involved in cell motility [1–3]. On the other hand, the clearest example of bacteria propulsion induced by actin polymerization is the well-studied *Listeria monocytogenes* [2, 4, 5], a variety of *Listeria* which has been linked to a number of fatalities by food poisoning [6]. When *Listeria* infects a host cell it exploits actin polymerization to move. Specifically bundles of actin form 'comet tails' which push the bacterium through the cytoplasm of the cell. *In vitro* experiments have also been performed substituting *Listeria* with artificial beads coated with WASP, which induced actin branching, comet formation and bead movement [7–9]. Besides confirming that actin polymerization was enough to account for the motility of those bacteria, these experiments are also useful to quantify the dependence of the bead velocity on parameters such as its radius, or the viscosity of the surrounding fluid [7, 8].

A successful model for polymerization-induced motility is the celebrated Brownian ratchet (BR) model introduced by Peskin *et al* in 1993 [10]. According to the BR model, the membrane or bacterium is represented as an obstacle which undergoes thermal diffusive motion. Such motion is random but can be rectified by the fibre modelled as an advancing straight rod. This model thus neglects the fibre elasticity; however, it is amenable to an analytic treatment which predicts a functional form for the velocity load curves (see section 2) that is in good semi-quantitative agreement with experiments [11]. The BR model has been generalized to the case of an elastic fibre [12], which itself undergoes thermal fluctuations. In this version the model is usually referred to as the elastic ratchet (ER). Now the obstacle motion can proceed via two distinct mechanisms: either by rectifying the obstacle diffusion or via bending of the fibre, which allows monomer intercalation and then straightening of the fibre as the obstacle moves. It may be expected, and has been shown [12], that an ER can push a diffusing obstacle more quickly than a corresponding BR. However, a quantification of the effect of tip fluctuations on the obstacle velocity versus load curves is hard within the semi-analytical treatment adopted so far and to our knowledge has not been attempted. Furthermore, giving the growing fibre a finite elastic modulus, or equivalently a finite persistence length, introduces another potential problem since the fibre can buckle or bend and lose its normal projection onto the obstacle. We do observe this phenomenon in our simulations, and are able to characterize its dynamics quantitatively. We call such a phenomenon a pushing catastrophe. It is important to stress that this problem is related to, but distinct from, the classical buckling problem, both in the Euler sense and in its more recent generalizations (see [13] and section 3), as in our case the fibre is growing and the wall is moving. Indeed, we find that, with physiological values for the ratio between polymerization and depolymerization rates, single actin fibres would undergo such a catastrophe with high probability. We discuss in section 4 what countermeasures the cell can take to render these catastrophes less likely [14].

The ratchet models have been further refined by a number of authors, who have considered more complete and realistic versions of the systems. For example a tethered ratchet model, in which the polymerizing fibre is at least transiently attached to the diffusing obstacle, has been proposed in [13, 15], and a better characterization of the obstacle as a fluctuating membrane has been attempted in [16, 17]. With few exceptions, these contributions have focused on analytically or semi-analytically tractable models. It would be desirable to study the same system via numerical simulations, which would then clarify the domain of validity of the analytical approximations. This is the programme which we follow in this paper.

We introduce a method to simulate numerically the three-dimensional dynamics of the growth of a semiflexible polymer against a fluctuating planar obstacle, modelling either a thermally diffusing bacterium such as *Listeria*, an artificial obstacle such as a portion of a polystyrene bead in a solution containing G-actin, with radius much larger than the polymer thickness, or a patch of the membrane of an eukaryotic cell with dimension smaller than the

typical 'mesh' size of a cellular membrane, i.e. around 100 nm [16]. The algorithm we use is a three-dimensional Monte Carlo (3D MC) dynamics, more specifically a generalization of a Monte Carlo procedure known as the 'kink-jump' algorithm which has recently been successfully applied to study dynamic effects in many polymer problems [17–24]. The choice of a stochastic Monte Carlo dynamics, versus for example a Langevin or molecular dynamics algorithm, is mainly dictated by convenience, as it naturally fits the stochastic nature of the growth rules typically used in the ratchet literature. Furthermore, it is much easier to implement hard constraints, such as those present between the wall and the fibre, in the ER model within a Monte Carlo scheme as opposed to a molecular dynamics simulation.

Our numerical results are used to test the velocity versus load curves predicted by the BR and ER model. There are only few related 'microscopic' simulations we are aware of: a simulation in two dimensions of a single growing elastic fibre [25], and the stochastic growth simulations in three dimensions of an infinitely stiff actin branched network [26]. Our simulations are three-dimensional and we quantify the velocity enhancement due to tip fluctuations. Moreover we study in detail the regime in which most fibres undergo what we call a 'pushing catastrophe', i.e. when the growth of the polymer becomes decoupled from the obstacle movement (see above). Beyond considering the basic elastic ratchet model, we also discuss two generalizations, one in which the wall becomes soft—mimicking a membrane patch—and another one in which the fibres are bundled via attractive interactions (e.g. via cross-linking) as occurs in filopodia in eukaryotic cells. We hope that our results will be of use in the design of more complicated models, for example representing a network of crosslinked semiflexible growing fibres, such as the actin cytoskeleton of eukaryotic cells, which will by necessity have to rely on more coarse grained models because of the large number of actin monomers taking part in the whole structure.

This work is structured as follows. In section 2, we introduce the ratchet models, define the quantities of interest in our work, and describe the Monte Carlo dynamic kink-jump algorithm used to generate our simulations. Section 3 presents a review of a selection of the semi-analytical results discussed in the literature on ratchet models, while section 2 contains the results of our simulations. In section 5 we draw our conclusions.

2. Model and simulation methods

In this section we introduce the model and the terminology used throughout this work, and we discuss the three-dimensional Monte Carlo dynamic algorithm employed to generate the numerical results presented in section 3. Our algorithm is akin to the one recently employed in different contexts in [20, 21], except for the fact that in our case the dynamics of the fibre is coupled to its growth via polymerization.

Figure 1 shows a schematic diagram of the system under consideration, together with the set of coordinate axes which will be used throughout. A semiflexible polymer, or fibre, is clamped at one end and is growing against a two-dimensional plane (obstacle) at the other end. The obstacle is parallel to the xy plane. The obstacle performs a random walk along the z axis with diffusion constant D_o. The semiflexible fibre is modelled by a (time-dependent) number, $N(t)$, of hard spheres of diameter h (labelled by their three-dimensional space positions $\{\vec{r}_i\}_{i=1,\ldots,N(t)}$), which are freely joined together by $N(t) - 1$ inextensible links of length a. We denote the link joining the ith and the $(i + 1)$th sphere $\vec{t}_i$. The state of the chain can equivalently be determined by specifying the azimuthal and polar angle θ_i and ϕ_i of each of the $N(t) - 1$ links (figure 1). In the continuum limit, θ, ϕ and $\vec{t}$ would become a function of a curvilinear length, s, which takes values comprised between 0 and $N(t)a \equiv L(t)$.

The model defined in figure 1 resembles the original ER model of [12]. The model parameters are: the polymerization and depolymerization rates at the free end, k_{on} and k_{off}

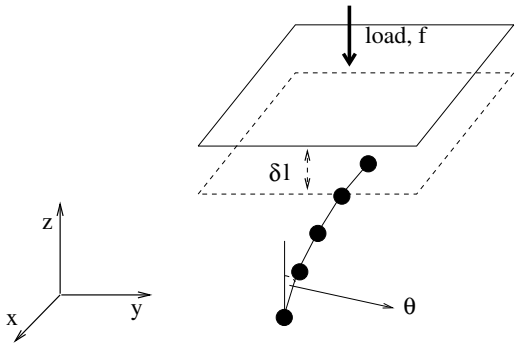

Figure 1. Geometrical set-up used for the three-dimensional dynamic Monte Carlo simulations. The symbols are defined in the text.

respectively; the clamping angle of the fibre at the origin, θ_1 ($\theta(s = 0)$ in the continuum limit) which we will denote by θ; the persistence length ξ of the fibre; the spatial diffusion coefficient of the obstacle D_o; the diffusion coefficient of the beads in the fibre which determines the angular diffusion coefficient of the fibre tip, D_t; and finally the load on the obstacle, which we identify with a downward pushing force f (see figure 1). The BR model is recovered if ξ tends to infinity, so tip diffusion can be neglected.

Typical values of the persistence length of actin fibres in eukaryotic cells are in the range 1–10 μm. Microtubules and sickle hemoglobin fibres are much stiffer than actin, so ξ is typically a few millimetres in these cases. Also bundles of actin fibres, such as those which comprise filopodia [27] *in vivo*, can to a first approximation be modelled as a single filament with a much enhanced stiffness with respect to a single actin fibre, so again the effective ξ is millimetres instead of micrometres (a more faithful description of filopodia taking into account all fibres in the bundle is presented in section 4 below). The polymerization dynamics can be controlled in experiments *in vitro* by varying the concentration of actin. In cells $k_{on} = 100\ s^{-1}$ and $k_{off} = 1\ s^{-1}$ [12]. In the simulations we consider two cases: one in which k_{off} is set to 0 (thus a good approximation for actin fibres in cells), and another one in which $k_{on}/k_{off} = 3$, to study length fluctuations close to the stalling force. Typical values for D_o vary greatly: for a patch of a membrane diffusion is very fast, $D_o \sim \mu m^2\ s^{-1}$, while the fluctuations of a whole bacterial cell are much slower: for a bacterium of μm size $D_o \sim 10^{-3}\ \mu m^2\ s^{-1}$. Also the load can vary: it is of the order of 1 pN when a consequence of the viscous drag of the fluid on the moving obstacle, while it can be larger than 50 pN for filopodia, which significantly deform the cellular membrane causing protrusion in the μm range. Tip fluctuations were quantified by an angular diffusion coefficient of $10^4\ rad^2\ s^{-1}$ in [12].

The numerical procedure we use is a dynamic Monte Carlo algorithm which evolves the system according to the following schedule: (a) the fibre is evolved by updating all the coordinates of the beads in it, or of $N(t)$ selected at random; (b) the obstacle position along z is updated; and (c) the fibre is elongated or shortened by a with probability proportional to the polymerization and depolymerization rates.

We discuss each of these three steps separately. First, we consider the update rule for the fibre. Technically, we simulate the dynamics of the semiflexible polymer using three-dimensional dynamic Monte Carlo kink-jump simulations. At each time step, we attempt to rotate a bead through a random angle—the bead is chosen randomly from those in the chain—around the axis joining its first nearest neighbours along the chain. The angle is chosen with uniform probability in the interval $[-\theta_0, \theta_0]$. If an end sphere is chosen, we rotate the terminal

link around a randomly chosen axis (chosen uniformly from the unit sphere) through a random angle in the $[-\theta_0, \theta_0]$ interval. Throughout the simulations θ_0 is a constant. If θ_0 is small enough this procedure is guaranteed to be equivalent to the generation of a Gaussian noise. However, we checked that the results were independent of θ_0. In particular $\theta_0 = \pi$ allows a larger time step, and we used this value in the simulations reported below. This choice is commonly made in dynamic studies with the kink-jump algorithm.

There is an interaction energy, H, between neighbouring spheres on the chain, which is due to the semiflexible nature of the fibres, and is given by

$$H = -K_{\mathrm{b}} \sum_{i=1}^{N-2} \vec{t}_i \cdot \vec{t}_{i+1} + V_{\mathrm{h.c.}}(|\vec{r}_i - \vec{r}_j|), \tag{1}$$

where $K_{\mathrm{b}} > 0$ is called the bending rigidity, and $V_{\mathrm{h.c.}}$ is the hard core potential, equal to ∞ if the distance between the centres of the ith and the jth beads is smaller than h. If $K_{\mathrm{b}} \gg 1$, the persistence length of the fibres, ξ, is $\sim K_{\mathrm{b}} a$. This Hamiltonian determines the dynamics through a standard Metropolis rejection test; at each trial move we compute the change in energy ΔH and accept the move with probability

$$W = \min\{\exp(-\beta \Delta H), 1\} \tag{2}$$

where $\beta = 1/(k_{\mathrm{B}} T)$, and k_{B} is the Boltmann constant which in our units is set to 1. We note that this scheme ensures that no chain intersection occurs *during* any attempted rotation of the links provided that the ratio between hard core diameter and bond length is large enough: precisely, one needs $h/a > (3/4)^{1/2} \sim 0.866$ [18]. We always use $h/a = 0.9$ in the simulations reported below.

We now consider the obstacle motion. The two-dimensional obstacle is fluctuating and its position along the z axis performs a random walk in time. We implement this by choosing with uniform probability a trial new obstacle position along z within a distance δl from the old one. If no load is applied then the obstacle simply undergoes Brownian motion, and it can be shown that the diffusion constant of the obstacle is $D_{\mathrm{o}} = (\delta l)^2/6$. If there is a load the obstacle performs a biased random walk, constrained by the presence of the fibre. This is implementing by adding a potential linearly increasing in z_{wall} to the system. In all cases we reject the trial position if any of the beads making up the fibre overlaps with the obstacle.

Finally, our simulation includes the polymerization dynamics. We model fibre growth by proposing an additional 'move' in our three-dimensional Monte Carlo dynamics: with probability k_{on} we attempt to add a monomer to the end of the fibre, i.e. attached to the monomer at $\vec{r}_{N(t)}$. The direction of the new link $\vec{t}_{N(t)}$ is chosen according to the probability distribution:

$$P(\vec{t}_{N(t)}) = \frac{\exp(\beta K_{\mathrm{b}} \vec{t}_{N(t)} \cdot \vec{t}_{\mathrm{N(t)-1}})}{\int \mathrm{d}\vec{t} \exp(\beta K_{\mathrm{b}} \vec{t}_{N(t)} \cdot \vec{t}_{\mathrm{N(t)-1}})}. \tag{3}$$

If the proposed new link crosses the obstacle position we reject the growth move. As the bending rigidity K_{b} is always very large in the cases considered here, this procedure is basically equivalent to choosing the new link in the direction of the last link of the already grown polymer, $\vec{t}_{\mathrm{N(t)-1}}$. Depolymerization is included by removing the monomer at the tip with rate k_{off}.

Time is measured in Monte Carlo steps. A Monte Carlo step is defined as a sequence in which, on average, all the beads in the polymer and the obstacle have had the possibility to move once [19]. It is possible to map in a straightforward way simulation units to real units by choosing a length scale, e.g. by fixing the monomer size a, and a timescale, which is set for example by specifying the obstacle diffusion constant. For more details on this point we refer the reader to [24].

3. A review on ratchet models and semi-analytical results

First, we review a selection of the literature on ratchet models and the semi-analytical predictions we compare with the simulations.

3.1. Brownian ratchet

First consider the BR model (i.e. the ER model in the limit $\xi \to \infty$), with the fibre normally incident to the obstacle. The BR model is equivalent to a one-dimensional system, in which the relative distance along z, which we call δz, from the tip of the straight fibre to the diffusing wall, is the only independent variable. The probability density for a distance δz at time t, denoted by $P(\delta z, t)$, obeys the following differential equation (see [10] for details, we neglect depolymerization, i.e. $k_{\rm off} = 0$):

$$\frac{\partial P}{\partial t} = D_{\rm o}\frac{\partial^2 P}{\partial \delta z^2} + \frac{D_{\rm o} f}{k_{\rm B}T}\frac{\partial P}{\partial \delta z} + k_{\rm on}\left[P(\delta z + a, t) - \Theta(\delta z - a)P(\delta z, t)\right]. \tag{4}$$

One can find a stationary equilibrium solution for P, from which the velocity force curves are determined as the implicit solution of the following system of equations (see also [10]):

$$\begin{aligned} v &= \frac{2D_{\rm o}}{a}\left[\frac{(\mu-\omega)\,\omega^2/2}{\omega^2 + (\exp(\omega) - 1 - \omega)\,\mu}\right] \\ \mu - \omega &= \frac{k_{\rm on}a^2}{D_{\rm o}}\left(\frac{1-\exp(-\mu)}{\mu}\right) \end{aligned} \tag{5}$$

where $\omega \equiv \beta f a = \frac{fa}{k_{\rm B}T}$. If the growing rod is advancing at an angle θ with respect to the diffusing wall, equation (5) still holds provided that a is substituted by $a\cos(\theta)$ everywhere. It is also useful to explicitly consider the limit of equation (5) for fast diffusion of the obstacle, i.e. $k_{\rm on} \ll \frac{D_{\rm o}}{a^2}$. In this limit, if we keep only the term of order 0 in a $1/D_{\rm o}$ expansion, we obtain

$$v = k_{\rm on} a \exp(-\beta f a). \tag{6}$$

Note that it is usually this limit which is fitted to experimental data. However, if $D_{\rm o}$ is not infinite the force should include a drag contribution from the viscosity of the fluid surrounding the obstacle. This is most easily seen by considering the solution up to terms of order $1/D_{\rm o}$ for large obstacle diffusion, and no external force (i.e. $\omega = 0$, see also [24]), when equation (5) becomes

$$v = \frac{2D_{\rm o}}{a}\frac{\mu}{1+\mu/2}, \tag{7}$$

and μ is given by the solution of the equation $\mu = \frac{k_{\rm on}a^2}{D_{\rm o}}\frac{1-\exp(-\mu)}{\mu}$. Expanding μ and hence v in powers of $1/D_{\rm o}$, and keeping only the terms linear in $1/D_{\rm o}$, we find that

$$\begin{aligned} \mu &\simeq \frac{\frac{k_{\rm on}a^2}{D_{\rm o}}}{1 + \frac{k_{\rm on}a^2}{D_{\rm o}}} \\ v &\simeq k_{\rm on}a\left(1 - \beta f_{\rm drag} a\right) \\ &\simeq k_{\rm on}a\exp(-\beta f_{\rm drag} a) \end{aligned} \tag{8}$$

where we have used the definition of drag force, i.e. $f_{\rm drag} = \beta v/D$ ($\beta = \frac{1}{k_{\rm B}T}$). Equation (8) clearly show that even for a large diffusion coefficient and in the absence of a load the tip cannot advance at the polymerization speed.

Another useful limit of equation (5) is when $k_{on}a^2 \gg D_o$, i.e. polymerization is much faster than diffusion. As $\frac{D_o}{k_{on}a^2} \to 0$, the wall velocity of a straight fibre becomes equal to [10]

$$v_{max,BR} = \frac{2D_o}{a} \tag{9}$$

which is known as the velocity of the ideal BR, and is in fact an upper bound for any D_o and k_{on}. The velocity of the ideal BR, given the values of D_o commonly accepted for *Listeria* [12], is too small to account for the experimentally observed speeds; hence the original rationale for introducing the ER model. Another obvious bound on the obstacle velocity, holding for both the BR and the ER models, is given by the polymerization rate k_{on} times a.

3.2. Elastic ratchet

In the ER model, the approximation that the fibre is infinitely stiff is relaxed, so the tip diffusion coefficient, D_t, is non-zero. In [12] it is shown that the tip flexibility can render the ratchet more quickly than predicted by the BR model. The original motivation to introduce the ER model was that experiments measuring the velocity versus load curve in bacteria propelled by actin showed little dependence on their size—and hence on the diffusion constant—(see [12, 15]). However, to our knowledge, no systematic analysis of the ER equations and in particular its increased speed obtained with respect to the BR model has been performed. Our numerical analysis (section 4.1, *Velocity laws*) provides a quantitative assessment of the dependence of the velocity on tip diffusion, incidence angle and persistence length.

Endowing the fibre with a finite elastic modulus, or, equivalently, with a finite persistence length introduces an additional issue: the fibre can bend or even buckle such that its polymerization direction no longer leads to obstacle movement. It is well known that for a straight fibre of fixed length L there is a buckling instability when subject to a compressional force equal to $f_b = \frac{\pi^2}{4}\frac{\xi}{L^2}k_BT$. Thus for a fibre incident at $\theta = 0$, there is a well-defined critical force: below f_b the fibre stays straight; for larger forces, the stable solution is one with a bent (buckled) fibre. As soon as the incidence angle is different from 0, this instability strictly speaking no longer exists (see appendix B in [24]). Thus, for any non-zero compressional force, the fibre bends and $\theta(s)$ is not constant along the fibre. However, for our problem of a growing fibre, it still makes sense to ask what is the maximum force the fibre can withstand before bending is so severe that the fibre grows parallel to the wall. When this happens, we will speak of a pushing catastrophe instead of buckling, because (a) the fibre is growing, i.e. out of equilibrium, and (b) the buckling instability strictly exists only for normally incident fibres. A semi-analytical calculation for the maximum force that an elongating fibre incident on a static (i.e. not diffusing) wall can sustain at an incidence angle θ has recently been performed [13], where the term buckling was used in a generalized sense (for the reasons outlined above we will not use this terminology here). The maximum force which a growing fibre can sustain, calculated in [13], can be accurately fitted via the formula

$$\frac{f_{max}d^2}{\xi k_BT} = A(90-\theta)^4 + B(90-\theta)^6 + C(90-\theta)^8 \tag{10}$$

where d is the distance between the clamping point of the fibre and the static wall, and with $A \simeq 8.4355\times10^{-8}$, $B \simeq -1.6403\times10^{-11}$ and $C \simeq 1.3055\times10^{-15}$. The discrepancy between this formula and the numerically determined relation of [13] is at most $\simeq$3% for θ between 0 and 60°. For normally incident fibres the 'buckling' instability is recovered (which is why the authors kept the nomenclature buckling for fibres incident at an angle). Equation (10) indicates that the maximum force is a steeply decreasing function of θ. As an example, if $\theta = 20°$, $\xi = 10$ μm and $d = 100$ nm, the maximum force the fibre can sustain at a temperature

$T = 300$ K is ∼3.5 pN, while for a straight fibre the buckling force in the same conditions is ∼10.2 pN.

3.3. Ratchet models with a fluctuating membrane

Finally, as mentioned in the introduction, while representing the obstacle as a fluctuating hard wall may be appropriate for a portion of an artificial bead or for a portion of a bacterium, it is problematic when applying the same ratchet models to a patch of a membrane because of its flexibility. A possible generalization of the ratchet model appropriate for the rectification of membrane motion has recently been suggested in [16] using statistical mechanics methods, at least in the case in which the fibre tip is normally incident on a membrane patch and the fibre is infinitely stiff. Such an approximation holds far from the buckling transition, and yields an explicit formula for the force, $f(z)$, felt by the fibre tip as a function of the tip position along z,

$$f(z) = 2\sqrt{A}\pi \frac{\exp(-Az^2)}{1 - \mathrm{erf}(\sqrt{A}z)} \tag{11}$$

where A is a parameter depending on the membrane elastic properties, which basically increases with the rigidity of the membrane, and $z = 0$ denotes the resting position of the membrane. It is to be stressed that the force in equation (11) is purely entropic, or equivalently comes from volume exclusion between the fibre and the membrane. Although far from the membrane the fibre tip still experiences a non-zero force, and the force is non-Hookean in that region, we can view equation (11) as equivalent to replacing a membrane with a 'soft wall', which penalizes configurations with the tip inside the 'membrane' with a potential:

$$V(z) = Az^2. \tag{12}$$

This formula gives the rationale for the generalization of the diffusing obstacle to a 'soft wall', which is presented in section 4—note however that in our case we consider the potential in equation (12) to hold for the mutual distance between the wall's instantaneous position and *any* points on the fibre, not just the tip. Typical values of $\sqrt{A}a$ for biological membranes are in the range 0.5–1.

4. Numerical results and comparison with analytical predictions

4.1. Velocity laws

In this section we estimate from our three-dimensional Monte Carlo dynamic simulations the velocity of the obstacle as a function of the imposed load. We consider semiflexible fibres with a persistence length of 2000 a, a polymerization rate $k_{\mathrm{on}} = 10^{-3}$, and consider two possible values for θ, 0 and 35° respectively. The rationale for this choice is that a normally incident fibre ($\theta = 0$) was originally considered in [10] as is typical in filopodia while $\theta = 35°$ is the optimal angle for a growing and branching network, such as observed in lamellipodia. The optimality of $\theta = 35°$ is a result of fibre branching occurring at a fixed angle of 70° under Arp2/3 [28]. Finally, we consider a range of possible values for the obstacle diffusion constant and the external load on the obstacle (see figure captions for their specific values).

To compute the obstacle velocity versus load curves, we averaged over several (typically 100) obstacle trajectories, and estimated the initial slope, i.e. before the fibre bends away from the obstacle. Similar methods were used in the numerical studies in [24, 25]. Figure 2 shows the velocity–force law for a series of simulations, with an incidence angle $\theta = 0$ (figure 2(a)) and 35° (figure 2(b)). Several remarks are in order here. First, the wall velocity is plotted against the *total* force, f_{tot}, acting on the obstacle, i.e. the external load plus the drag force. Second,

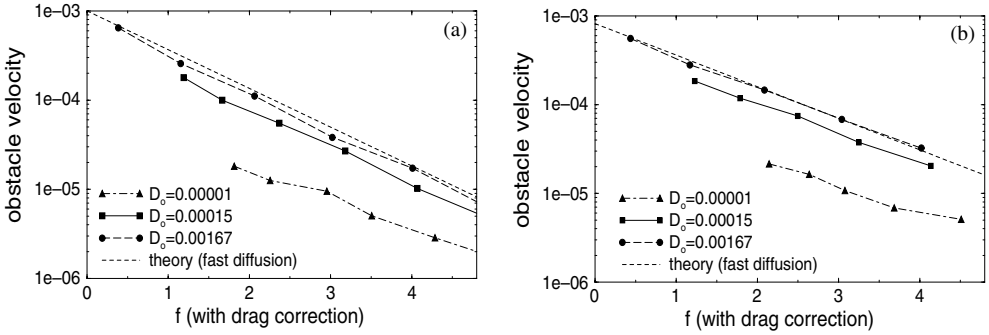

Figure 2. Wall velocity versus load force law (in linear–logarithmic plot) for $\theta = 0$ (a) and $\theta = 35°$ (b). Parameters are: $k_{on} = 10^{-3}$, $k_{off} = 0$, $\xi = 2000\ a$, and D_o as shown in the legend. The force includes the drag force contribution and are measured in units of $k_B T/a$. Other quantities are measured in simulation units.

for both incidence angles there is an increasing deviation from the conventional velocity–force relation $v \sim \exp(-\frac{fa}{k_B T})$ as the obstacle diffusion constant decreases. The fast diffusion limit is shown in figure 2 for comparison. More specifically, our data suggest an approximate law of the kind $v = A \exp\left(-\frac{f_{tot} a}{k_B T}\right)$ to hold, with $0 < A < 1$ a prefactor which depends on D_o. Third, one can perceive the effect of changing the incidence angle by comparing figures 2(a) and (b). While the qualitative trends are similar, the deviation from the fast diffusion limit are smaller for the oblique fibre at the same value of D_o. The data corresponding to the oblique fibre (figure 2(b)) show some evidence of a slightly larger slope (in the linear logarithmic plot) than the one predicted by the ratchet models, which may result from the fact that 35° is a non-optimal angle and bending away from 35° can enhance the obstacle speed. In [12] it is shown that 45° is the optimal angle to maximize the obstacle velocity.

Finally, it is interesting to ask whether in our simulations the velocities observed are mainly due to rectifying the fluctuations of the obstacle as in the BR model or those of the filament tip as in the ER model, as both mechanisms are in principle viable and incorporated in our numerics. From figure 2 it is already clear that the tip fluctuations cannot fully compensate in the case of slow obstacle diffusion, so for $D_o \sim 10^{-3}\ \mu m^2\ s^{-1}$, or below, the obstacle velocity falls much below the polymerization speed $k_{on} a$ even in the absence of an external load. Mapping our simulation parameters to physical values, tip fluctuations in the Monte Carlo dynamics are in the physical range for actin tips. We have also performed simulations in the *adiabatic* limit, in which, before moving the obstacle via thermal diffusion, we perform a large number of Monte Carlo moves for the fibre, so effectively the tip diffusion is much enhanced (ideally infinitely fast with respect to the other timescales, set by the obstacle diffusion and polymerization). Even in this extreme case, we do not see significant deviations from the curves in figure 2.

A quantitative estimate of the contribution of the tip fluctuations to the obstacle velocity can be obtained by subtracting from the velocity–load curves the prediction for the BR model (see section 3 and [10]). As the BR model considers an infinitely stiff polymer, the predicted velocity is simply due to rectifying the obstacle thermal diffusion, and thus it will be smaller than the one observed in our simulations. The extra velocity we observe is then entirely due to the tip fluctuations. Figure 3 shows such a comparison, for $D_o = 1.67 \times 10^{-6}$ (in simulation units), and parameters as above—so this is valid for a fibre with actin-like persistence length. The velocity of the obstacle is only slightly larger than the BR prediction in the normal incident case, and on average ∼40% higher for the oblique fibre case.

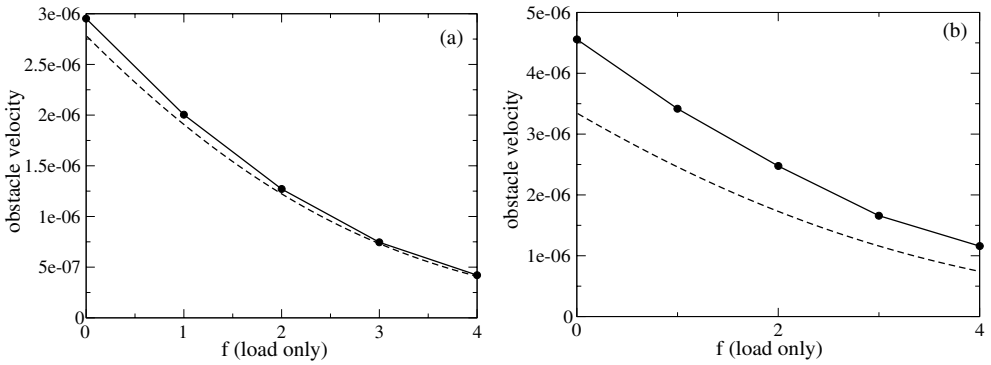

Figure 3. Comparison between the velocity versus load curves obtained with the three-dimensional Monte Carlo dynamics and the predictions from the BR model. Parameters are $D_o = 1.67 \times 10^{-6}$, $k_{on} = 0.001$, $k_{off} = 0$, $\xi = 2000a$, while the incidence angle is $\theta = 0$ in (a), and $\theta = 35°$ in (b). The forces do not include the drag force contribution and are measured in units of $k_B T/a$.

4.2. Pushing catastrophes

As explained in section 3 (see *Elastic ratchet*), there are two main differences between the BR and ER models. First, tip fluctuations can push the obstacle more effectively, although our numerics suggest that this effect is not dramatic. Second, as the fibre is growing against a wall with a non-zero load (which includes the drag force), there will be a maximum, length-dependent, force that it can sustain before it bends away from the obstacle. As the depolymerization rate is zero, we also note that whatever the force the fibre can never stall (see section 4.3, *Modifying the polymerization dynamics*) and its ultimate fate will be to undergo a 'pushing catastrophe', an example of which is shown in figure 4(a). Once again we stress that we denote the phenomenon sketched in figure 4(a) as a catastrophe, reserving the term buckling to the classical Euler buckling instability. When a fibre undergoes a catastrophe it is practically impossible for it to recover the straight configuration (favoured by the bending rigidity potential) since unhindered polymerization rapidly extends the fibre. In other words, the fibre growth and the obstacle movement become uncorrelated.

The occurrence of catastrophes is linked to the classical analysis performed in [13], but our simulations suggest that they are also of a stochastic nature. In particular we determine the probability that a catastrophe occurs at time t, (figure 4(b)) for a normally incident fibre and a persistence length of $500a$. In order to define a time in which a catastrophe occurs we have used the following operational definition. We define a catastrophe as a divergence of the trajectories in the $(z(t), N(t))$ plane (the two variables denote respectively the instantaneous wall position and fibre length at time t) from the ideal curve corresponding to the case in which growth is coupled to wall movement. For a threshold condition, we define a catastrophe event when $\frac{z(t)-N(t)\cos(\theta)}{N(t)\cos(\theta)}$ becomes larger than 0.3, where θ is the fibre clamping angle; see figure 1.

From figure 4(b) it can be seen that as the load on the obstacle increases, the mean of the catastrophe time distribution increases and the distribution broadens. These distributions for the catastrophe times may be useful when designing more coarse grained models for the dynamics of one or more growing fibres pushing an obstacle (although when considering many interacting ratchets recovery can be more likely than for a single ER fibre; see also section section 4.4, *Bundling the fibres* below). If fibres are obliquely incident, as expected from the classical analysis in [13], catastrophes occur sooner.

We close this section with a discussion of the implications of our results to cellular cytoskeletal dynamics. In the cytosol of eukaryotic cells the polymerization rate is around

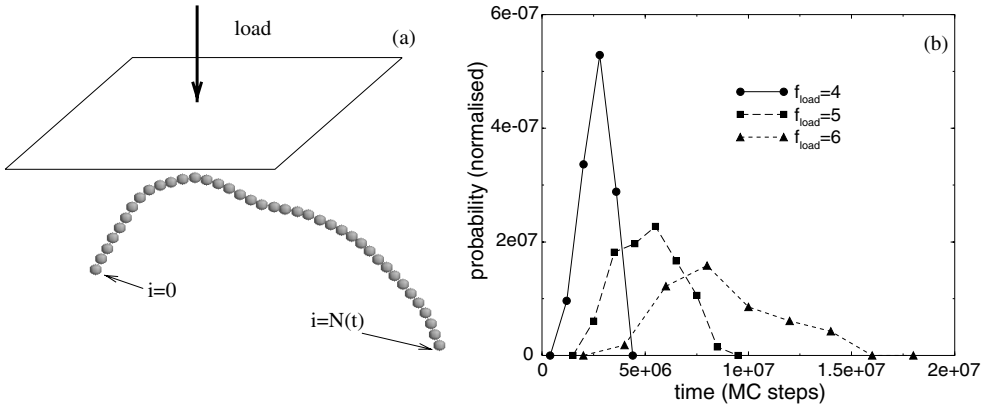

Figure 4. (a) Example of a fibre that has undergone a pushing catastrophe in our simulations. (b) Time distribution probabilities for catastrophes for a fibre with $\xi = 500a$ and $\theta = 0$ under different loads (in the legend in units of $k_B T/a$) found by averaging 90 different simulations. We used $D_o = 1.67 \times 10^{-5}$, $k_{on} = 10^{-3}$ and $k_{off} = 0$.

two orders of magnitudes larger than the depolymerization rate, so neglecting k_{off} as here is a good approximation for actin fibres in living cells. Further, the force exerted by a cellular membrane is easily in the pN range, so actin fibres in cells should undergo a pushing catastrophe with high probability. While this is true for some of the fibres, typically the older ones or those far from the cellular membrane, actin fibres at the leading edge of a moving cell are typically pointing forward and actively pushing the membrane via polymerization. Why then do all actin fibres in a cell not undergo a pushing catastrophe sooner or later? The answer seems to be that cells have taken 'precautions' for this not to occur. First, there are capping proteins which bind to the barbed end of an actin fibre and inhibit further growth [2, 29], so the average length reached by an actin fibre at the leading edge of the cell is ∼50–100 nm (∼20 beads in our simulations). Second, there are cross-linking proteins which can merge several actin fibres into a single thicker and much stiffer bundle, which can grow against a large external force. This strategy is used to create filopodia [27]. Third, at least some of the fibre tips appear to be tethered to the membrane, possibly in a transient way [13, 15], and this should also render catastrophes less likely.

4.3. Modifying the polymerization dynamics

Although in eukaryotic cells the polymerization rate is thought to be significantly larger than the depolymerization rate, because of an excess concentration of monomeric G-actin, in *in vitro* experiments the ratio k_{on}/k_{off} can be tuned at will. This introduces another phenomenon, specifically stalling and its associated stalling force. To analyse stalling, consider a mean-field theory for a ratchet model at large obstacle diffusion so that the rate of polymerization is not diffusion limited. According to the BR and ER at large diffusion, an external load reduces polymerization by an exponential factor in $\frac{fa}{k_B T}$, while leaving k_{off} unaltered. Therefore in the mean-field approximation the growth of a straight fibre ($\theta = 0$) can be described by the following continuum differential equation for the instantaneous fibre length, $L(t)$:

$$\frac{\partial L(t)}{\partial t} = a\left[k_{on}\exp(-\beta f a) - k_{off}\right]. \tag{13}$$

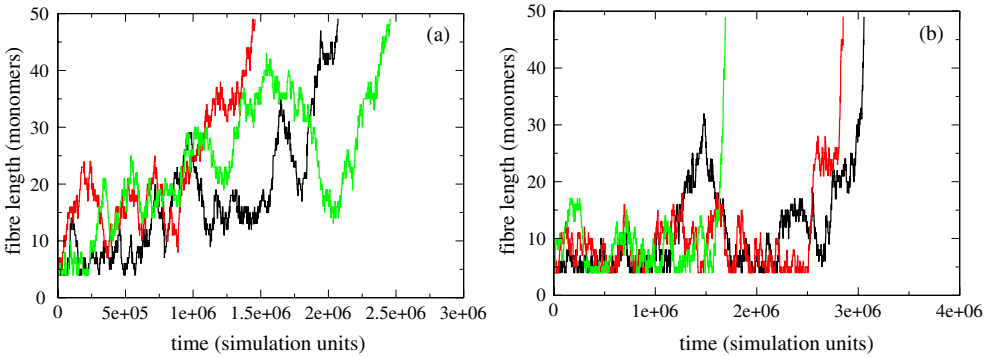

Figure 5. Three typical time series for fibre length of a fibre with $k_{on} = 0.001$, $k_{on}/k_{off} = 3$, persistence length (a) $\xi = 2000a$ and (b) $\xi = 200a$, and an obstacle with $D_o = 1.5 \times 10^{-4}$ and a load equal to (a) 1 and (b) 1.2 in units of $k_B T/a$, which are close to the stalling force, $f_s \sim 1.1$.

It is straightforward to deduce that fibre growth ceases or stalls when the external force equals the critical load $f_s = k_B T \frac{\log(k_{on}/k_{off})}{a}$. If the fibre is growing at an angle θ to the wall, then the stalling force is given by $f_s = k_B T \frac{\log(k_{on}/k_{off})}{a \cos(\theta_{tip})}$, where θ_{tip} is the angle between the fibre tangent at the tip and the normal to the wall (the z axis in our simulations).

We have simulated the growth of a straight fibre with $k_{on} = 10^{-3}$, and $k_{on}/k_{off} = 3$ to probe the effect of a finite depolymerization rate on fibre growth and obstacle motility. If we approximate θ_t with the initial clamping angle, θ, which will be valid for $L(t) \ll \xi$ and far from a pushing catastrophe, then the stalling force in our units is $\log(3) \simeq 1.0986$. Below stalling, without an applied load, the velocity is still well defined, although smaller than in the case with no depolymerization, as predicted by the BR and ER models. Above stalling, on the other hand, e.g. $f \geqslant 2$, the fibre fails to grow during the whole simulation time, which corresponds to several seconds, as predicted by equation (13).

Our simulations reveal an interesting dynamics close to the stalling force. Figure 5 shows three typical realizations of the time series for the length of a growing fibre against the diffusing wall under a load which is just below (figure 5(a)) or just above (figure 5(b)) the stalling force $f_s = \log(3)$. In both cases the fluctuations are very large, both when considering the semiflexible fibre and the stiff one (Brownian limit). In part this is due to the fact that the polymerization is stochastic, and close to stalling large excursions should be expected. A factor which amplifies length fluctuations in the elastic fibre is that temporary tip fluctuations can lead to faster growth when the fluctuations lead to a larger angle between fibre tip and wall normal. Another point to note is that, when the stalling force is smaller than the force on the obstacle, a catastrophe might still eventually occur, provided that the difference between f and f_s is small. This can be clearly seen in figure 5(b), with $f = 1.2 > f_s$, where it can be seen that there is a 'stalling plateau' in which the fibre grows and shrinks, followed by a steep increase corresponding to a catastrophe. Note that for $f \geqslant 2$, this phenomenon is no longer observed during our simulations, which span a time of several seconds, because in this time the fibre length is too small to allow the fibre to achieve a sufficient curvature to escape. The stochasticity of growth and the coupling between tip fluctuations and growth are out of the reach of mean-field treatment of equation (13).

The behaviour displayed by the simulations of figure 5 is reminiscent of the dynamic instability of microtubules [2], a less dramatic version of which has also recently been discussed for actin fibres *in vitro* [30]. Usually these dynamic instabilities are explained by invoking the

presence of ageing of monomers in the fibre, through hydrolysis of the ATP molecules bound to actin monomers and tubulin dimers, to ADP, so that typically close to the tip there is a 'cap' of ATP-rich monomers which ensures growth, and the loss of the cap via a fluctuation drives the dynamic instability. Our dynamics is phenomenologically similar to this and experiments with fibres under a load would be useful to discriminate between the instabilities due to the loss of ATP caps and those highlighted here.

4.4. Bundling the fibres

Actin fibres in eukaryotic cells are sometimes bundled together, e.g. via crosslinks whose formation is favoured by the fascin protein. Typically this bundling occurs when filopodia, the finger-like protrusions at the leading edge of a moving cell, are formed [27]. The most apparent advantage of fibre bundling is that, as specified above, the bundle becomes considerably stiffer than the single fibre. This is quantified as an increase in the persistence length or the fibre bundle, denoted ξ', with respect to that of a single actin fibre, $\xi \sim 10\ \mu$m. The physical association between fibres in the bundle determines the relative increase in stiffness (see [2] for details). First, a bundle built via loosely associating n fibres allows the filaments to slide against each other as they bend, and therefore the persistence length increases linearly with n—or with the square of the bundle radius. We note that this scaling is similar to the case of the persistence length of the tubes considered in [31] for double-stranded DNA inside a phase capsid. At the other extreme, links between the filaments can be so strong that the bundle behaves practically as a single thicker filament and thus $\xi' = n^2\xi$ (the persistence length of a filled tube of thickness Δ increases with the fourth power of Δ [2]). The real situation is in between, although recent simulations [32] of a realistic bundle of actin fibres modelling a filopodium suggest that the second scenario is more appropriate, and a law of the kind $\xi' \simeq n^2\xi/2$ has been fitted to the data. Due to the enhanced rigidity, bundles can endure a larger force and it is harder for them to undergo buckling or a catastrophe. A second advantage of bundling is that the step size decreases on average by a factor of n, while the ratio between $k_{\rm on}$ and $k_{\rm off}$ is identical to that of a single fibre, so the stalling force also increases linearly in n. To summarize, bundles of fibres close to the membrane are harder to bend, buckle or stall than a single fibre, and this possibly explains their use in exploratory cell movement as filopodia.

From a modelling point of view, the ER model can describe a bundle of n fibres as well as a single fibre, in a mean-field approximation, provided that we substitute $K_{\rm b}$ with $K_{\rm b}n^2$ (assuming strong cross-linking between the fibres in the bundle), $k_{\rm on}$ with $nk_{\rm on}$, $k_{\rm off}$ with $nk_{\rm off}$, and a with a/n. In particular, we can find the velocity versus load curves for a bundle of n BRs ($\xi = \infty$), for the case $k_{\rm off} = 0$, via equation (5), provided we scale $k_{\rm on} \to nk_{\rm on}$ and $a \to a/n$. Note that this scaling leaves the polymerization velocity $k_{\rm on}a$ unchanged. Figure 6 shows how the velocity versus load curves change for a single fibre and a bundle of n fibres. It can be seen that, if the diffusion constant is small, so a single fibre cannot proceed at polymerization speed, bundling the fibre can increase the velocity. Since the velocity depends on $\frac{fa}{k_{\rm B}T}$, the velocity of a bundle is also predicted to be less sensitive to load force.

Figure 7 shows the results of a series of direct Monte Carlo simulations of 20 growing fibres with actin-like parameters (for a list of all the parameters see the caption to figure 7), subject to different interactions between the fibres. The fibre origins were initialized randomly in a small disc, so that the packing was close to maximum, and the orientations of all fibres were initially normal to the fluctuating wall. We have considered three cases: first when the fibres were not interacting, second when they were interacting only via self-avoidance, and finally when there is an attractive potential between beads (whether on the same or different fibres). The attractive potential was chosen as a square well with depth ϵ, hard core at a mutual

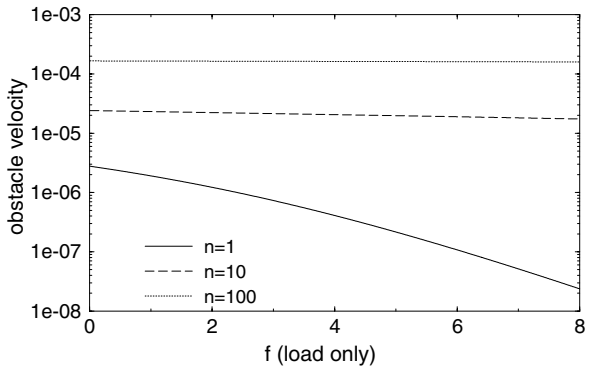

Figure 6. Effect of fibre bundling within the BR model. We plot the velocity versus load curves for a bundle of n Brownian ratchets, with $k_{\rm on} = 10^{-3}$, $k_{\rm off} = 0$, and $D_{\rm o} = 1.5 \times 10^{-6}$. Solutions are found by using equation (5) and scaling parameters for a single fibre as discussed in the text. The forces do not include the drag force contribution and are measured in units of $k_{\rm B}T/a$.

distance of h and range Δr. We have taken typically $\Delta r = 0.6a$, which is of the order of a few nm, and varied ϵ between 0 and 20 $k_{\rm B}T$. All three cases lead to a faster movement of the obstacle with respect to both the BR and the ER prediction for a single fibre. This enhancement (of order 5) is, however, smaller than the ideal 20-fold enhancement predicted via naively mapping a into a/n as above.

It is noticeable that the presence of many fibres leads to a larger velocity (see figures 7(A) and (B), conformation (I)), even when they are not interacting. This is because there is a distribution of possible gaps between fibre tips and obstacle at any time and intercalation is thus more likely (effectively a is smaller) while all n fibres provide rectification of the obstacle diffusion. Moreover, the simultaneous presence of many fibres renders pushing catastrophes less frequent. A typical conformation of 20 non-interacting fibres growing against a fluctuating wall is shown in figure 7(B), conformation (I). For comparison with conformations (II) and (III), we have set the origins of the fibres close together although the distance between the fibres does not affect the results in this case. If the fibres interact through self-avoidance only, the fibres tend to grow straighter than n unconstrained fibres and we find a similar velocity increase—as compared to the unconstrained case—with respect to the BR prediction. Monomer intercalation is hampered by steric effects and we believe this is why the obstacle moves more slowly. Endowing the fibres with an attractive bundling interaction renders the structure unstable as the fibres twist or tilt with respect to each other. While this self-interaction is certainly of use in stiffening the fibres, it does not lead to a faster obstacle motion. Paradoxically, if the interaction is too strong, some of the fibres cannot grow because an aggregate of fibres has blocked their polymerization (no capping was included in the simulations). This is why the number of fibre tips in figure 7 (configuration (B III), which corresponds to $\epsilon = 20\ k_{\rm B}T$) is smaller than 20.

4.5. Softening the obstacle

Here we consider the case of a soft wall potential between fibre and obstacle, suggesting this may be a reasonable model for a fluctuating and diffusing membrane. Instead of simply excluding the configurations where the fibre crosses the obstacle, as was done with the hard wall simulations reported thus far, we penalize them with a potential (A and B are two positive

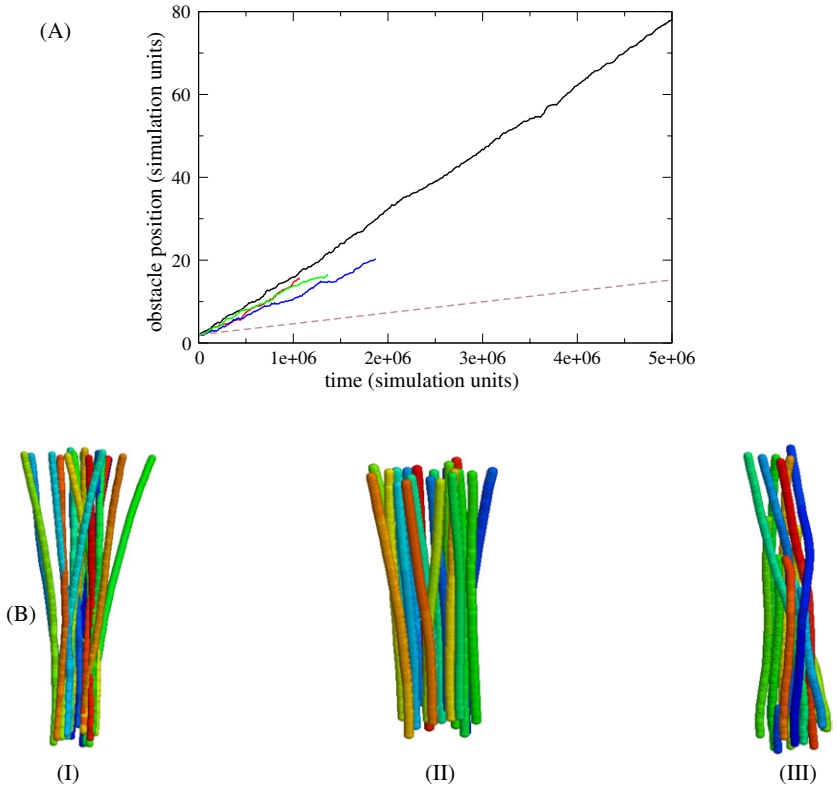

Figure 7. Effect of bundling 20 fibres studied by 3D MC simulations. Parameters are: $D_o = 1.67 \times 10^{-6}$, $k_{on} = 0.0033$, $k_{off} = 0$, $\xi = 2000\ a$, $\theta = 0$, and $f = 0$. (A) Time series of the obstacle position. From top to bottom, curves refer to a single simulation for: 20 non-interacting fibres (black), 20 fibres with self and mutual steric avoidance (red), and two examples of fibres with attractive bundling interactions with $\epsilon = 10$ (green) and 20 (blue) $k_B T$. The long dashed line gives the Brownian ratchet limit. (B) Typical configurations of (I) 20 non-interacting fibres shown as a group for simplicity (each fibre should be spatially separated as they do not interact), (II) 20 fibres with self and mutual steric avoidance, and (III) a bundle of 20 fibres with bead–bead interaction of 20 $k_B T$ (see text).

constants):

$$V_{soft} = \sum_{i=1}^{N(t)} A|z_i - z_{wall}|^B \Theta\,(z_i - z_{wall}) \tag{14}$$

where z_{wall} and z_i are the position along the z axis (figure 1) of the obstacle and the ith bead respectively and Θ is the Heaviside step function. Increasing A and B both render the wall harder. We focus on the case $B = 2$, which can be derived from excluded volume interaction between a fibre and a membrane for small membrane deformation (section 3). We chose a value of A so that $\frac{\sqrt{A}a}{k_B T} = 1$, which is reasonable for biological or cellular membranes. Figure 8 shows the different velocity versus load curves for the soft wall and the excluded volume wall ($A = \infty$), for $\theta = 0$ and two different values of D_o. The BR limiting behaviour is also shown. For the larger obstacle diffusion constant (figure 8(a)), the soft wall moves only slightly more quickly than the hard (excluded volume) wall and the BR. Figure 8(b) instead shows that, when D_o is small, while the excluded volume wall moves only slightly more quickly than the BR,

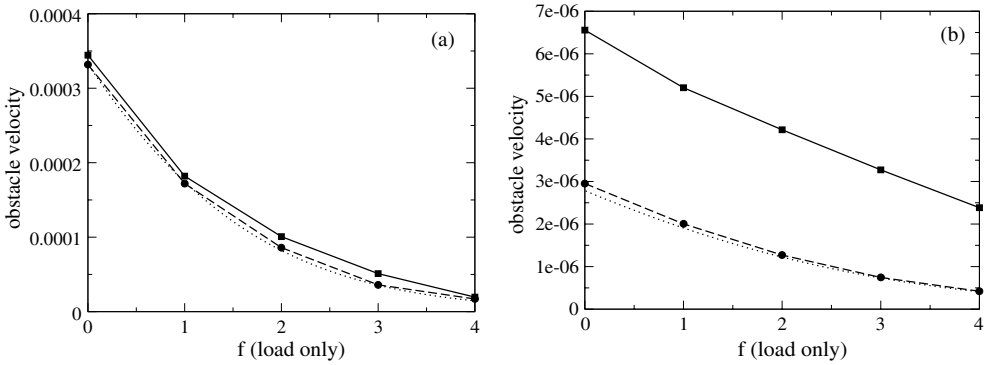

Figure 8. Comparison between the velocity versus load curves obtained with the three-dimensional Monte Carlo dynamics for the soft and the hard wall, and the predictions from the BR model. Parameters are: $k_{\rm on} = 0.001$, $k_{\rm off} = 0$, $\xi = 2000\,a$, $\theta = 0$. For the soft wall we chose $\frac{\sqrt{Aa}}{k_{\rm B}T} = 1$ and $B = 2$ (see text). $D_{\rm o}$ was 4.2×10^{-4} in (a) and 1.5×10^{-6} in (b). The forces do not include the drag force contribution and are measured in units of $k_{\rm B}T/a$. For both (a) and (b), the dotted curve refers to the BR prediction, the long-dashed one the hard wall result, and the solid line to the soft wall curve.

the velocity of the soft wall is significantly larger. In other words the wall moves more quickly as it is softened. This can be qualitatively understood by noting that the obstacle now moves in a repulsive potential created by the fibre, in contrast to the previously independent motion except for intermittent collisions with the fibre (in the hard wall case).

We note that when the wall becomes 'soft', we also need to modify the rule for fibre growth. In our simulations we have assumed that if the proposed position for the newly grown bead (the $N(t)$th) is within the obstacle, we accept this move with probability $\exp(-\epsilon)$, where

$$\epsilon = \frac{a_1 |z_{\rm wall} - z_{N(t)}|^{a_2}}{k_{\rm B}T}. \tag{15}$$

We anticipate that other rules may lead to different obstacle velocity laws.

5. Discussion and conclusions

We have presented a numerical method to investigate the dynamics of a growing fibre, or a set of fibres, close to a diffusing obstacle. The algorithm we use is a generalization of the three-dimensional kink-jump Monte Carlo dynamics originally introduced in [18]. Its main advantage in our application is that it naturally fits with the stochastic nature of the dynamics governing fibre growth and obstacle diffusion. Moreover, by introducing branching and capping probabilities [26], our algorithm may naturally be generalized to study the dynamics of a whole network of actin fibres, although our full treatment (bead-by-bead) of the polymer relaxation will render it suitable only for rather small networks.

Through simulations, we have mapped the velocity versus load curves for a fibre with physical properties close to that of an actin fibre, and we have shown that the fluctuations of fibre tip can render the elastic ratchet faster than the Brownian one in the case of slow obstacle diffusion, although the increase is not dramatic (of the order of 40–50% at most in the cases considered here and in [24]).

We also highlighted two novel mechanisms under which the obstacle can move more quickly than predicted by a simple (Brownian or elastic) ratchet model. One is via fibre

bundling, or more simply when there are multiple polymerizing fibres directed towards the obstacle: the obstacle speed then increases because heterogeneities in the instantaneous states of the fibres lead to a smaller effective gap between tip and obstacle. Another mechanism is through softening of the wall, i.e. in the case in which the wall is not infinitely rigid but has a 'width' in which the fibre tip can enter: a possible physical realization of this system may occur via a fluctuating membrane [16].

We have also indicated that if the ratio between the polymerization and the depolymerization rate is large, as is typical for actin fibres in living cells, then polymers with the stiffness of actin will typically undergo a pushing catastrophe and grow away from the cellular membrane when they have grown too long, more than a few tens of monomers in our simulations. While this can occur, it is by no means a common fate to all fibres in an eukaryotic cell: indeed the cell seems to have taken 'precautions' to reduce the frequency of catastrophes. These include the recruitment of capping proteins, and the bundling of fibres via cross-linking proteins, which effectively stiffens the actin fibres.

Finally, our stochastic model suggests that tuning the thermodynamic stalling force to be close to the load on the obstacle—by modifying the polymerization kinetics—leads to interesting dynamics, in particular to large fluctuations in the fibre length and to some degree of correlation between stochastic fluctuations and fibre tip instantaneous position. These phenomena may be observable in controlled *in vitro* experiments.

Acknowledgments

We acknowledge valuable discussions with D R Daniels and M S Turner. This work was supported by EPSRC grant GR/S29256/01.

References

[1] Alberts B *et al* 2003 *Molecular Biology of the Cell* 4th edn (New York: Garland)
[2] Bray D 2000 *Cell Movements: From Molecules to Motility* 2nd edn (New York: Garland)
[3] Stossel T 1993 *Science* **260** 1086
[4] Zeile W L, Zhang F, Dickinson R B and Purich D L 2005 *Cell Motil. Cytoskeleton* **60** 121
[5] Shukarev V *et al* 1995 *Cell Motil. Cytoskeleton* **30** 229
[6] Philadelphia Department of Public Health 2002 *Outbreak of Listeriosis Northeastern United States* Public Health Dispatch
see also Ivins M and Dubose L 2003 *Bushwhacked* (New York: Random House) chapter 8
[7] van der Gucht J, Paluch E, Plastino J and Sykes C 2005 *Proc. Natl Acad. Sci. USA* **102** 7847
[8] van Oudenaarden A and Theriot J A 1999 *Nat. Cell. Biol.* **1** 493
[9] Wiesner S *et al* 2003 *J. Cell. Biol.* **160** 387
[10] Peskin C S, Odell G M and Oster G F 1993 *Biophys. J.* **65** 316
[11] Janson M E and Dogterom M 2004 *Phys. Rev. Lett.* **92** 248101
[12] Mogilner A and Oster G 1996 *Biophys. J.* **71** 3030
[13] Dickinson R B, Caro L and Purich D L 2004 *Biophys. J.* **87** 2838
[14] Howard J 2001 *Mechanics of Motor Proteins and the Cytoskeleton* (Sunderland, MA: Sinauer)
[15] Mogilner A and Oster G 2003 *Biophys. J.* **84** 1591
[16] Daniels D R and Turner M S 2004 *J. Chem. Phys.* **121** 7401
[17] Satyanarayana S V M and Baumgartner A 2004 *J. Chem. Phys.* **121** 4255
[18] Baumgartner A and Binder K 1979 *J. Chem. Phys.* **71** 2541
[19] Baumgartner A 1980 *J. Chem. Phys.* **72** 871
Baumgartner A 1984 *Annu. Rev. Phys. Chem.* **35** 419
[20] Muthukumar M 2001 *Phys. Rev. Lett.* **86** 3188
[21] Chern S-S, Cardenas A E and Coalson R D 2001 *J. Chem. Phys.* **115** 7772
[22] Kantor Y and Kardar M 2004 *Phys. Rev.* E **69** 021806

[23] Marenduzzo D *et al* 2002 *Phys. Rev. Lett.* **88** 028102
[24] Burroughs N J and Marenduzzo D 2005 *J. Chem. Phys.* **123** 174908
[25] Carlsson A E 2000 *Phys. Rev.* E **62** 7082
[26] Carlsson A E 2001 *Biophys. J.* **81** 1907
[27] Svitkina T M *et al* 2003 *J. Cell. Biol.* **160** 409
[28] Maly I V and Borisy G G 2001 *Proc. Natl Acad. Sci. USA* **98** 11324
[29] Rafelski S M and Theriot J A 2004 *Annu. Rev. Biochem.* **73** 209
[30] Vavylonis D, Yang Q B and O'Shaughnessy B 2005 *Proc. Natl Acad. Sci. USA* **102** 8534
[31] Marenduzzo D and Micheletti C 2003 *J. Mol. Biol.* **330** 485
[32] Mogilner A and Rubinsten B 2005 *Biophys. J.* **89** 782